Ultrastable iridium-ceria nanopowders synthesized in one step by solution combustion for catalytic hydrogen production

Thanh-Son Nguyen, Georgeta Postole, Stéphane Loridant, Françoise Bosselet, Laurence Burel, Mimoun Aouine, Laurence Massin, Patrick Gélin, Franck Morfin, and Laurent Piccolo

Electronic Supplementary information

A. Experimental Section: Characterization

The concentrations of iridium and chloride were determined using inductively coupled plasma optical emission spectroscopy (ICP-OES, Activa instrument from Horiba Jobin Yvon). In order to dissolve them completely, the samples were treated with a mixture of H_2SO_4, royal water and HF at 250-300 °C.

Isotherm and specific surface area measurements were performed by N_2 adsorption volumetry at -196 °C using the BET method (ASAP 2010M instrument from Micromeritics). Prior to surface area determination, the powders were outgassed at 300 °C for 2 h in vacuum.

Thermogravimetric measurements combined with differential thermal analysis and mass spectrometry (TG-DTA-MS) were performed with a Setsys Evolution-1200 instrument from Setaram coupled with a mass spectrometer (Omnistar from Pfeifer) through a capillary system. The experiments were performed by heating 15 mg of the sample located in a 100 µL Pt crucible from RT up to 900 °C with a heating rate of 5 °C min^{-1} under argon flow (50 mL min^{-1}). The MS was set at specific m/z values in order to follow the possible formation of H_2, H_2O, N_2, NH_3, NO_x, O_2, CO, CO_2, C_2H_4, CH_2N, $C_2H_5NO_2$, $CNCH_3$, Cl_2, HCl, and CH_3Cl.

The crystalline structure was analyzed with two different powder X-ray diffractometers (XRD). For RT measurements at ambient atmosphere, a Bruker D8 Advance A25 diffractometer (Cu Kα radiation at 0.154184 nm) equipped with a Ni filter and 1-D fast multistrip detector (LynxEye, 192 channels on 2.95°) was used. The diffractograms were collected at 2θ with steps of 0.02° from 4 to 80 ° for a total acquisition time of 32 min and from 20 to 85° for a total acquisition time of 110 min. For *in situ* XRD

measurements, the diffractometer employed was a Panalytical X'Pert Pro MPD equipped with a diffracted beam graphite monochromator (Cu Kα radiation at 0.154184 nm) and 1-D fast multistrip detector (X'Celerator, 127 channels on 2.1°), using the Bragg-Brentano flat plate geometry. The samples were mounted in an atmosphere-controlled Anton Paar XRX 900 reactor chamber. The temperature-regulated glass-ceramic sample holder was open to allow hydrogen flowing through the sample (20 mL min^{-1}). Heating was performed up to 750 °C at a rate of 2 °C min^{-1} and 0.5 hour dwell time was observed before XRD data collection (20-85° 2θ range, 0.033° 2θ steps, 158 min per scan). Phase identification was performed using the Diffrac.Eva software (Bruker) and the ICDD-PDF4+ database. The lattice parameters and the crystallite sizes were determined by the Rietveld method (Fullprof code).[1]

The sample microstructure was also examined by scanning electron microscopy (SEM) and high-resolution transmission electron microscopy (HRTEM). The SEM images were obtained from a Jeol JSM 5800LV microscope (W filament, 3.5 nm resolution, operating voltage 15 kV), while the HRTEM pictures were recorded under high-vacuum mode using a FEI Titan aberration-corrected ETEM operating at 300 kV with 1 Å best resolution. For TEM, the samples were crushed in ethanol and the solution was ultrasonically stirred before dropping on a holey carbon-covered copper TEM grid and lamp drying. For SEM, the samples were poured as thin layers on double-sided adhesive carbon discs on the sample holder, and metalized with gold to avoid charging.

X-ray photoelectron spectroscopy (XPS) was carried out with a KRATOS AXIS Ultra DLD spectrometer equipped with a magnetic immersion lens, a hemispherical analyzer and a delay line detector. The base pressure in the analysis chamber was 5 10^{-10} mbar. All the data were acquired using a monochromated Al K$_\alpha$ X-ray source (1486.6 eV, 150 W), at a normal angle with respect to the surface. The analyzer was operated at 160 eV pass energy for acquisition of survey scans and at 20 eV pass energy for acquisition of high-resolution spectra of Ce 3d, Ir 4f, C 1s and O 1s core levels. Charge neutralization was used to compensate charging of the samples and the area analyzed was 700 μm × 300 μm. The spectra were referenced to the 3d$^{3/2}$ peak of Ce^{4+} at 916.0 eV binding energy. Before surface analysis, the samples were heated to 400 °C for 2 h under H$_2$ flow or at 300 °C for 1 h under O$_2$ flow (50 mL min^{-1}, 1 atm) in an *in situ* high-temperature quartz reaction cell. For obtaining the Ce$_2$O$_3$ sample (Ce^{3+} reference), a CeO$_2$ sample (A sample, Table 1) was calcined *ex situ* in air at 400 °C for 3 h, reduced *in situ* in H$_2$ at up to 700 °C, and sputtered with Ar$^+$ ions for 1 h in the UHV preparation chamber. The Shirley background correction was applied, and the spectra for Ir 4f core levels were peak-fitted using 30 % Lorentzian-to-Gaussian functions. For Ce 3d core levels, a fitting procedure using a linear combination of CeO$_2$ and Ce$_2$O$_3$ spectra obtained on our samples was used (see main text and Fig. S7).

Raman spectra of the samples were recorded with a LabRam HR Raman spectrometer (Horiba-Jobin Yvon) equipped with BXFM confocal microscope, interference and Edge filters, and charge-coupled device detector. The exciting line at 514.5 nm of an argon laser (CVI Melles Griot) was focused using a ×50 long-working-distance objective. The spectra collected using diffraction grating of 1800 grooves per mm were accurate within 1 cm^{-1}. Typical Raman spectral collection times were 80 s (20 s per scan and 4 scans per spectrum). The Raman spectra were calibrated using the Si 521 cm^{-1} shift, and normalized over the main peak area. All the recorded data were initially treated using the LabSpec software (Horiba-Jobin Yvon).

Infrared spectroscopy of adsorbed CO was performed with a Thermo Nicolet 6700 FTIR spectrophotometer equipped with an *in situ* diffuse reflectance infrared Fourier Transform spectroscopy (DRIFTS) chamber (Harrick HVC-DRP cell) and a high-sensitivity MCT detector. The cell was connected to a gas handling system allowing for *in situ* treatments with several gases at temperatures up to 500 °C. About 30 mg of the powder sample was placed into the cell sample holder and pretreated *in situ* under He flow (40 mL min^{-1}, 1 atm) at 300 °C for 1 h. CO was pre-adsorbed by exposing the sample kept at 50 °C to a flow of 1% CO in He for 15 min. Then the CO+He feed was replaced by pure He, and a spectrum was acquired at 50 °C. For reduction, the sample was exposed to a flow of pure H_2 at 400 °C for 1 h. The spectra were recorded in the 650-4000 cm^{-1} range at a resolution of 2 cm^{-1} by accumulating 128 scans. The Omnic software (Thermo) was used for initial data processing.
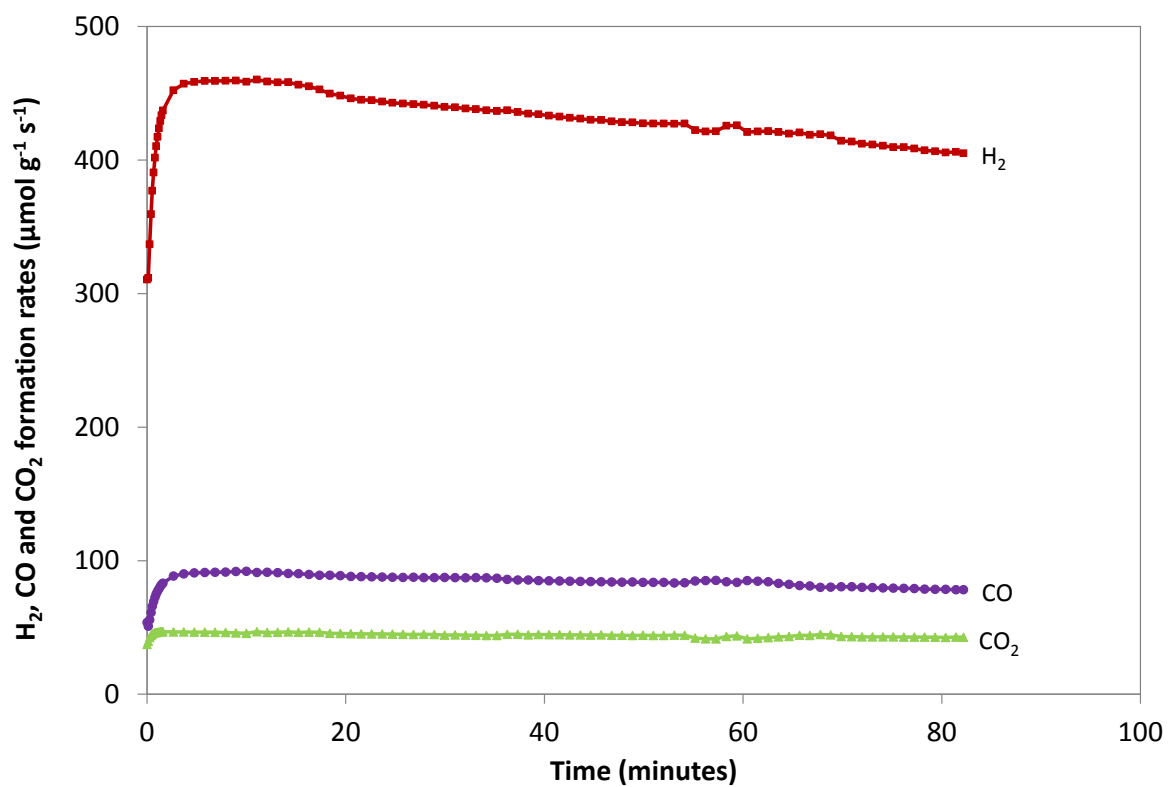
B. N₂ volumetry
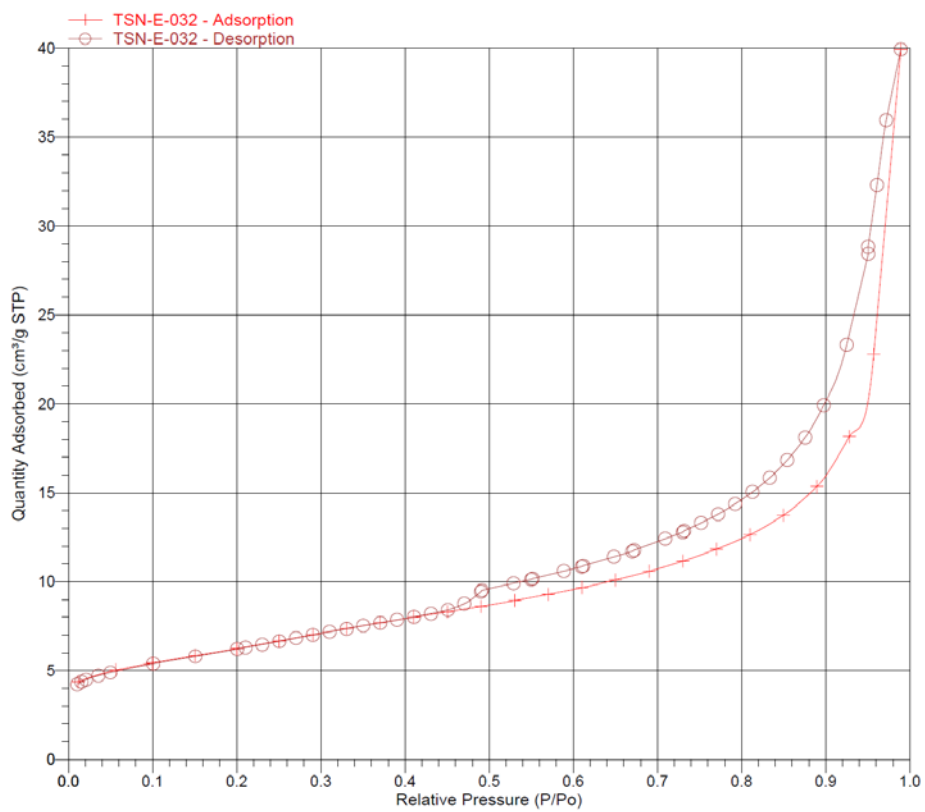
Fig. S1. N$_2$ adsorption/desorption isotherm of CeO$_2$(A).

C. Catalytic tests

Table S1. Product formation rates for three testing times (these data correspond to those reported in Fig. 1a). $\eta_{WGS} = P_{CO2}P_{H2}/P_{CO}P_{H20}K_{eq,WGS}$, with $K_{eq,WGS}$ = 1.31 at 750°C. $K_{eq,WGS}$ is the equilibrium constant of the water-gas shift reaction ($CO + H_2O \rightarrow CO_2 + H_2$).

| Catalyst	Product formation rates ($\mu mol\ g^{-1}\ s^{-1}$)			CH_4 consumption rate ($\mu mol\ g^{-1}\ s^{-1}$)	η_{WGS} (-)
	H_2	CO	CO_2		
CeO$_2$(A)					
1h	2.63	0.21	0.50	0.71	
8h	2.74	0.22	0.52	0.74	
16h	2.71	0.21	0.52	0.73	0.12
0.11 wt% Ir-CeO$_2$-SCS					
1h	771	203	40	244	
9h	796	216	37	253	
16h	813	224	35	259	1.09
0.33 wt% Ir/CeO$_2$-IWI					
1h	761	232	16	249	
9h	742	225	16	243	
16h	717	219	15	235	0.60

Fig. S2. Long-term activity test of the Ir-CeO$_2$-SCS catalyst.

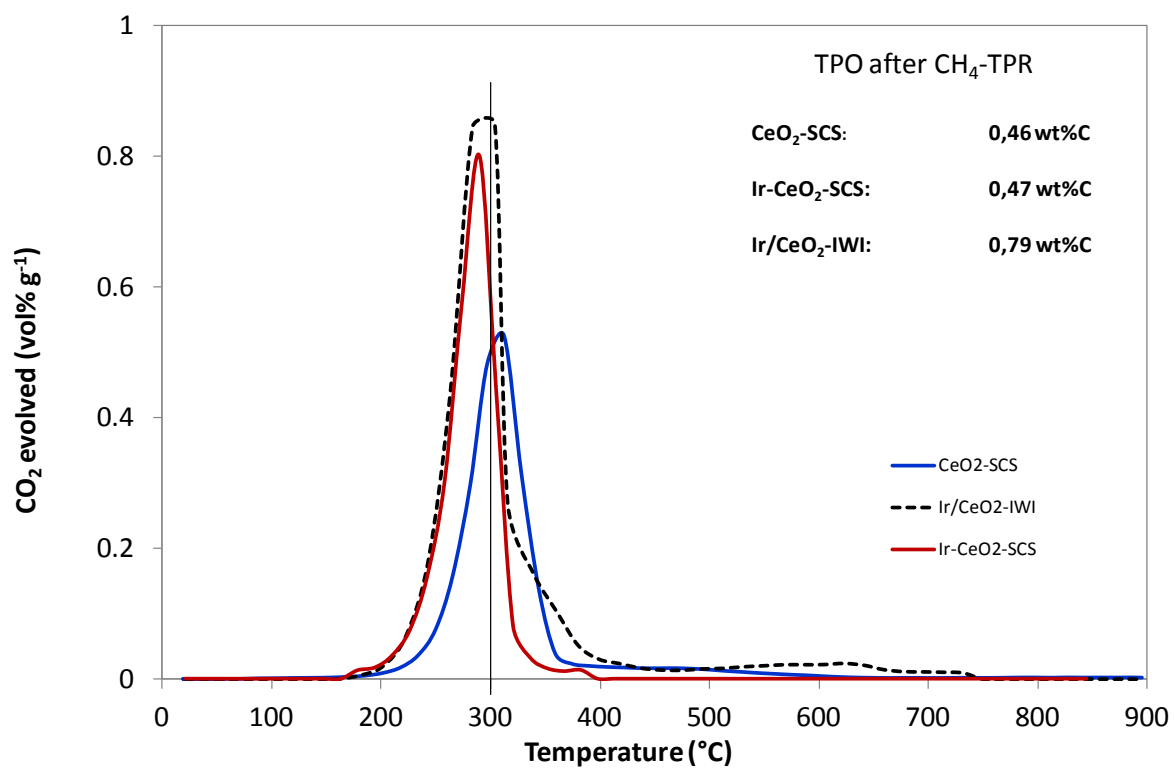**D. Temperature-programmed experiments**
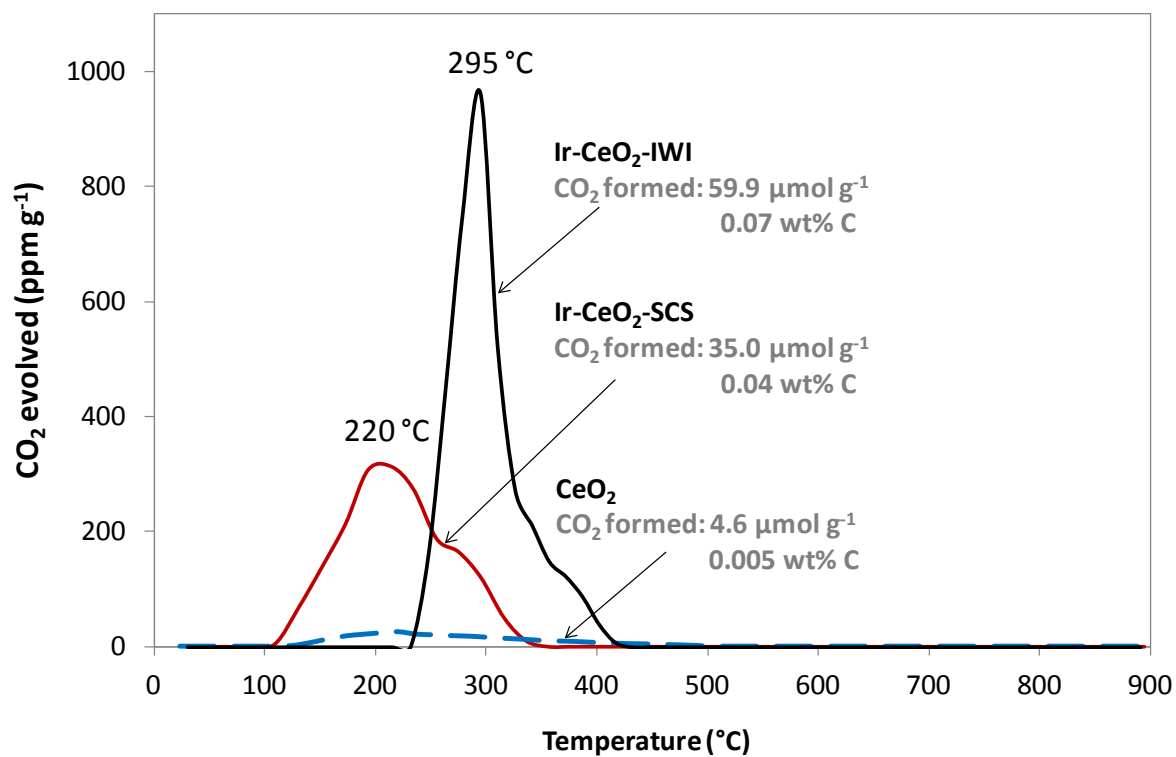
Fig. S3. Evolution of CO_2 during TPO runs performed after the SRM tests of Fig. 1a. The total amounts of CO_2 formed are indicated, as well as the corresponding amounts of carbon.
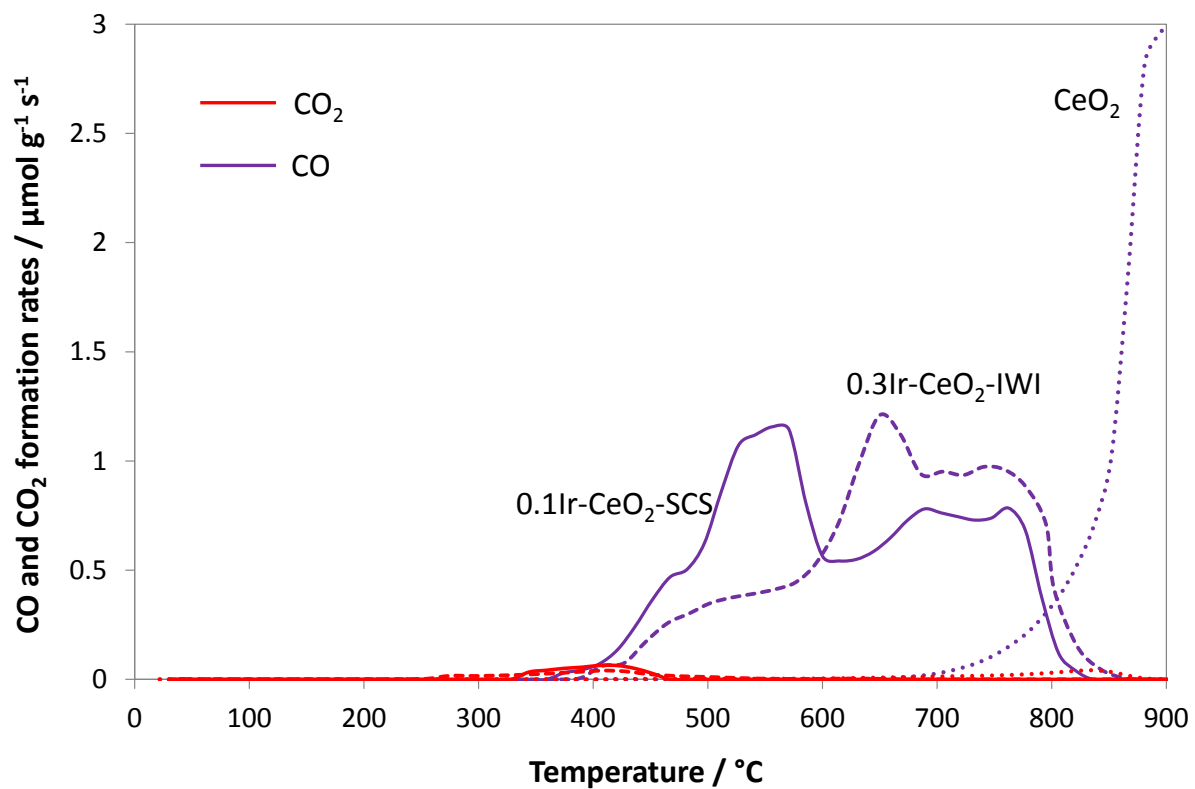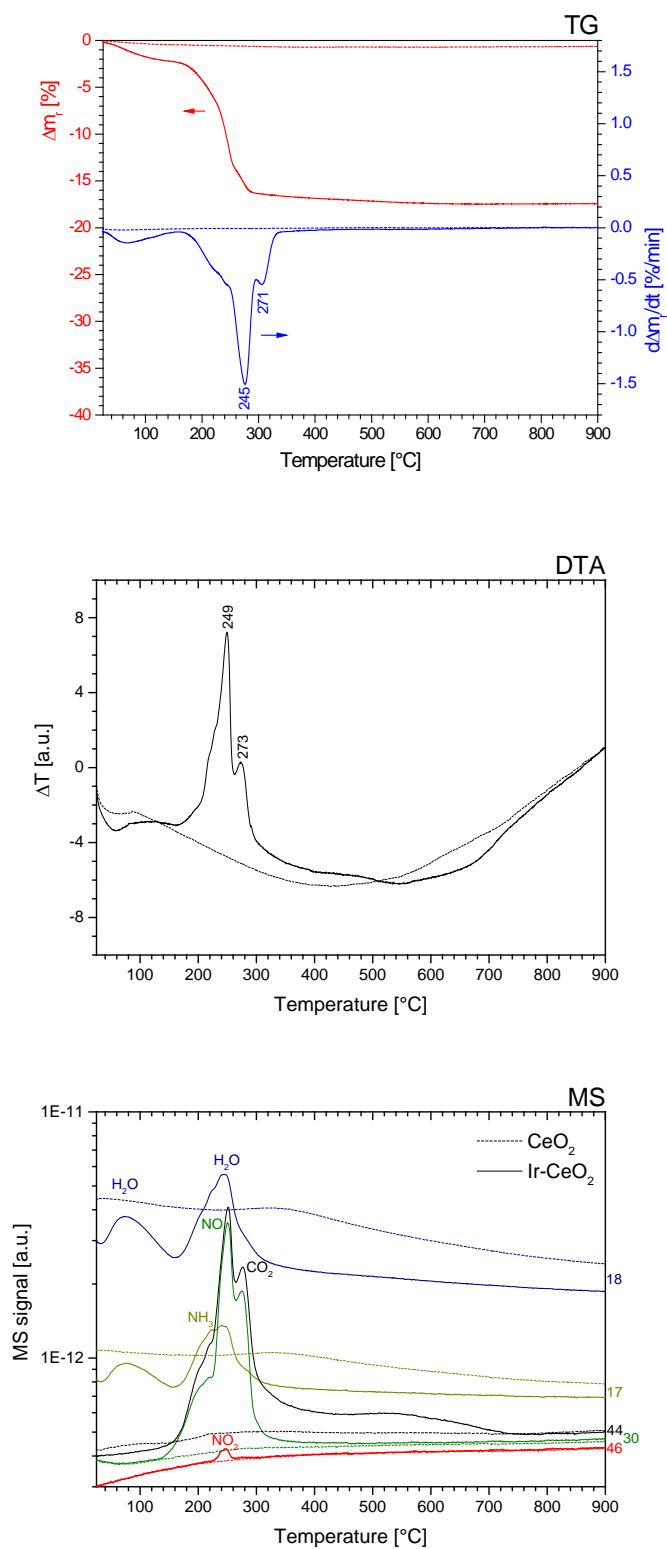
Fig. S4. CO and CO_2 desorption rates during CH_4-TPR of the catalysts. The H_2 signal is not shown for clarity (see Fig. 1b).
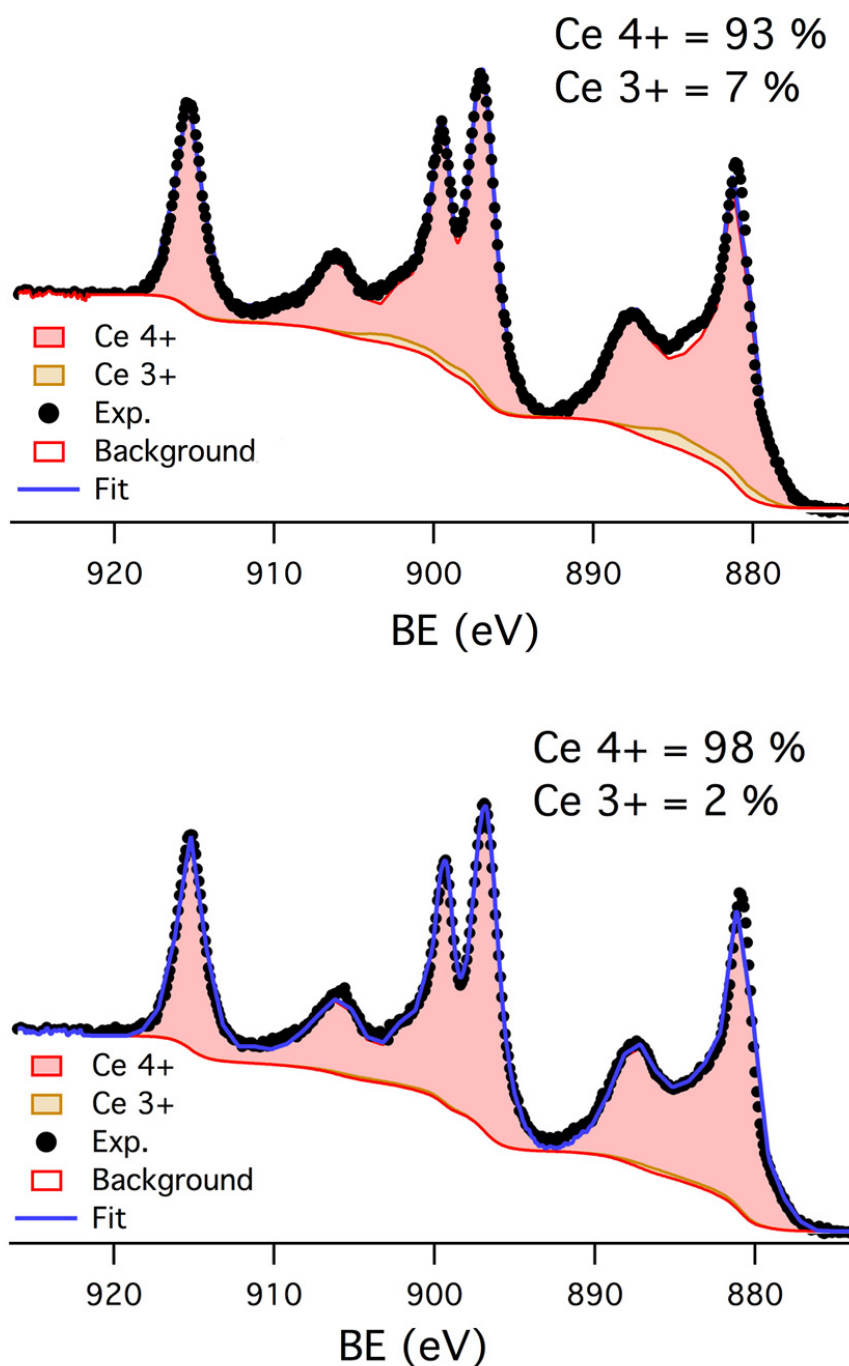
Fig. S5. Evolution of CO_2 during TPO runs performed immediately after the corresponding CH_4-TPR runs of Fig. S4. The amounts of reacted carbon are indicated.

E. Thermogravimetry

Fig. S6. Simultaneous TG-DTA-MS experiments on CeO$_2$ (·····) and Ir-CeO$_2$ (–). Conditions: N$_2$ atmosphere, 5 °C min^{-1}, 50 mL min^{-1}, 15 mg. See Ref. 2 for details.

F. X-ray photoelectron spectroscopy

Fig. S7. XPS spectra (Ce 3d core levels) for Ir-CeO$_2$-SCS (top graph) and Ir/CeO$_2$-IWI (bottom graph) submitted to reducing treatments. The numerical fits from a linear combination of reference CeO$_2$ ("Ce 4+") and Ce$_2$O$_3$ ("Ce 3+") spectra are shown. These spectra were recorded on pre-calcined and Ar$^+$-sputtered ceria, respectively (see Section A and main text).

References

1. The Fullprof program and documentation can be obtained at http://www.ill.eu/sites/fullprof, .
2. G. Postole, T. S. Nguyen, M. Aouine, P. Gélin, L. Cardenas, and L. Piccolo, Appl. Catal. B, 2014, **submitted**.